Electronic Supplementary Material (ESI) for Journal of Materials Chemistry A.

Supporting Information:

Engineering Multi-Chambered Carbon Nanospheres@Carbon as Efficient Sulfur Hosts for Lithium-Sulfur Batteries

Authors:

Shikui Wu,*[a] Qun Cao [a], Minjie Wang [b], Tengfei Yu [a], Huanyun Wang [a] and Sha Lu[b]

Affiliations:

[a] College of Pharmacy, Inner Mongolia Medical University, No.5 Xinhua west street, Hohhot 010059, PR China. *E-mail: shikuiwu@yahoo.com, Fax:+86 04716653172, Tel: +86 04716653172.

[b] School of Basic Medicine, Inner Mongolia Medical University, No.5 Xinhua west street, Hohhot 010059, PR China.

Table S1. Electrochemical performance comparison of MCCN@C material with the representative sulfur host in literatures [17,26,28,30-39].

Ref.	Sulfur hosts (morphology)	Sulfur percentage (wt.%)	Sulfur loading mass (mg cm^{-2})	Rate performance	Capacity at 1.0 C after cycling	Capacity at 2.0 C after cycling	Cycling stability
This work	MCCN@C	83.1	1.1	626 mAh g^{-1} at 5.0 C	810 mAh g^{-1} after 1,000 cycles	651 mAh g^{-1} after 1,000 cycles	0.032% per cycle
36	Carbon nanocages	79.8	1.0–1.5	--	580 mAh g^{-1} after 300 cycles	--	0.042% per cycle
45	Nitrogen-doped hollow carbon nanospheres	85.0	0.5–0.7	250 mAh g^{-1} at 2.0 C	--	--	0.12% per cycle
47	N-doped hollow porous carbon bowls	--	1.0	535 mAh g^{-1} at 4.0 C	706 mAh g^{-1} after 400 cycles	--	0.053% per cycle
51	3D graphene nanosheet@carbon nanotube	70.0	1.1–1.5	409 mAh g^{-1} at 2.0 C	364 mAh g^{-1} after 500 cycles	--	0.09% per cycle
52	N-doped graphene-carbon nanotube	62.8	1.1	458 mAh g^{-1} at 5.0 C	629 mAh g^{-1} after 1000 cycles	495 mAh g^{-1} after 1000 cycles	0.031% per cyle
53	N-doped double-shelled hollow carbon spheres	62.0	3.9	430 mAh g^{-1} at 3.0 C	--	--	0.19% per cycle
54	Hierarchical Carbon Nanotubes	50.0	0.8–1.0	696.5 mA h g^{-1} at 1.0 C	558 mA h g^{-1} after 150 cycles	--	0.13% per cycle
55	MWNTs into hollow porous carbon nanotubes	71.0	--	550 mAh g^{-1} at 3.0 C	647 mAh g^{-1} after 200 cycles	--	0.089% per cycle
56	Graphitic carbon nanocages	77.0	--	765 mA h g^{-1} at 5.0 C	706 mA h g^{-1} after 1000 cycles	--	0.0215% per cycle
57	Activated porous carbon nanotube	75.0	2.2	857 mAh g^{-1} at 5.0 C	--	--	0.09% per cycle
58	Reduced graphene oxide/Co-doped porous carbon polyhedrons	51.0	1.0	359 mAh g^{-1} at 5.0 A g^{-1}	--	--	0.03% per cycle
59	hierarchical porous graphene/Fe_2O_3	60.0	1.0	565 mAh g^{-1} at 5.0 C	--	380 mAh g^{-1} after 500 cycles	0.09% per cycle
60	Polypyrrole-MnO_2 coaxial nanotubes	70.0	2.0	350 mAh g^{-1} at 4.0 C	550 mAh g^{-1} after 500 cycles	--	0.07% per cycle

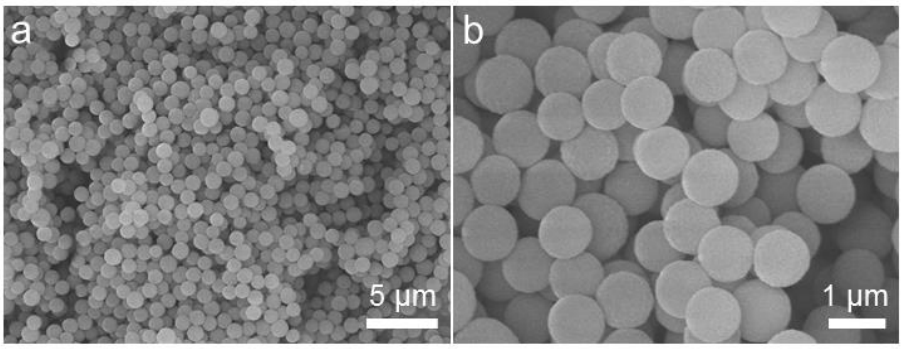

Fig. S1. SEM images of the metal-based precursor, showing the uniform size distributions.

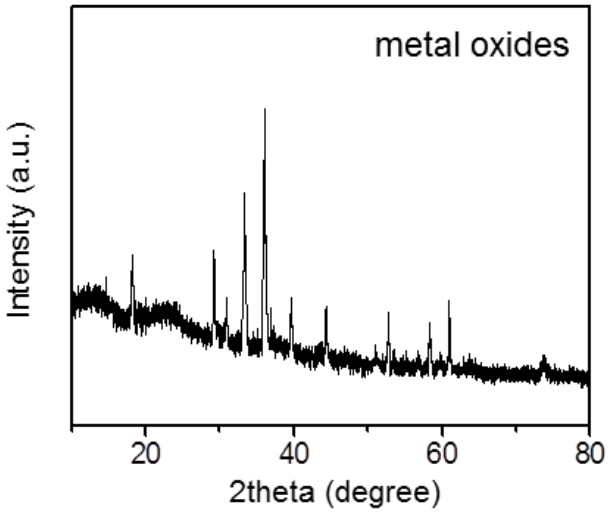

Fig. S2. XRD pattern of metal oxides, showing the diffraction peaks corresponding to $CoMn_2O_4$ (JCPDS card, No. 77-0471).

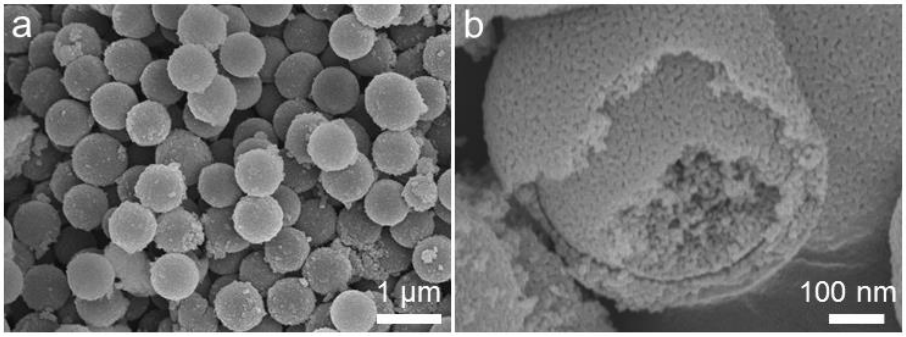

Fig. S3. (a,b) SEM images of metal oxides. The image in (a) indicates the spherical morphology of metal oxides, and the image in (b) suggests the presence of pores inside the metal oxides.

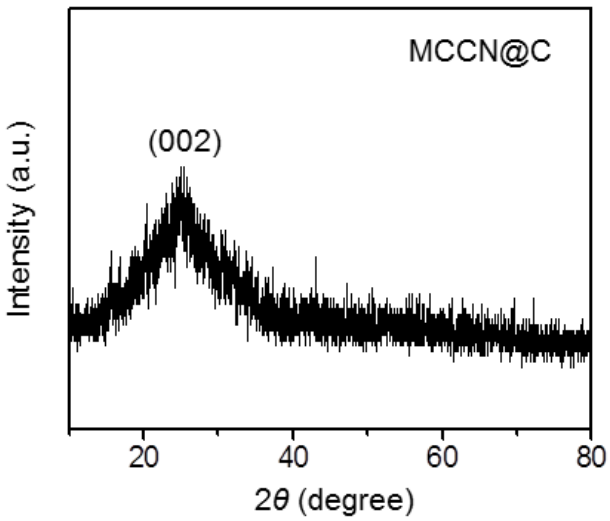

Fig. S4. XRD pattern of MCCN@C material, revealing the moderate graphitic degree of carbon material.

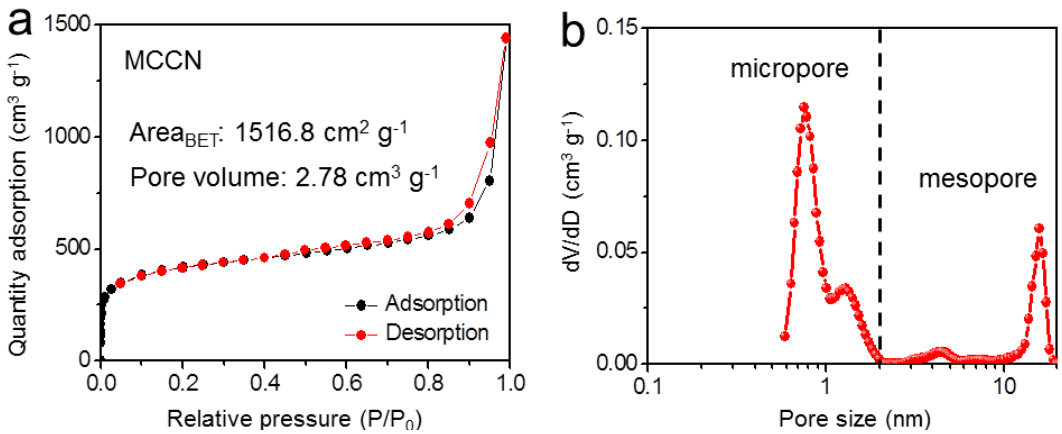

Fig. S5. Surface area and pore size distribution of MCCN material. (a) N_2 adsorption-desorption isotherms and (b) pore size distribution curve of MCCN material. The characterization reveals a typical micro-mesoporous characteristic with high surface area of 1516.8 cm^2 g^{-1} for MCCN material. The micropore sizes center at 0.75 and 1.30 nm, and the mesopore sizes locate 4.42 and 15.6 nm.

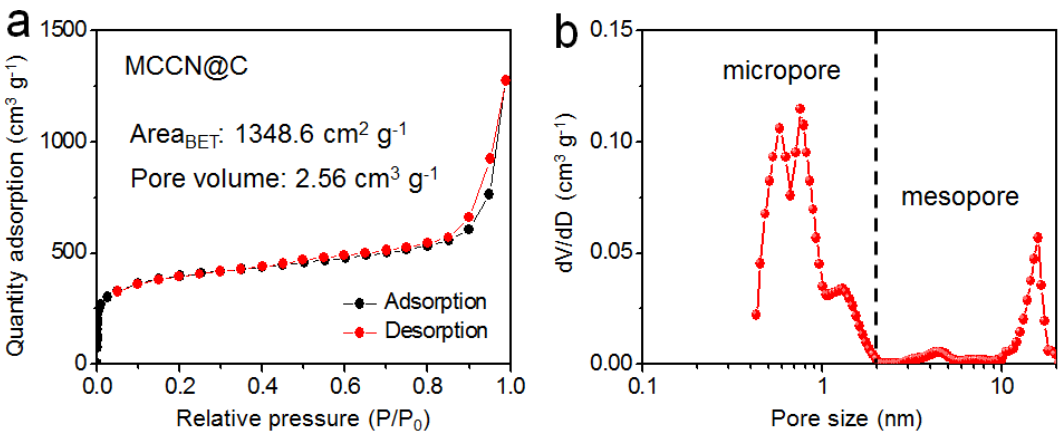

Fig. S6. Surface area and pore size distribution of MCCN@C material. (a) N_2 adsorption-desorption isotherms and (b) pore size distribution curve of MCCN@C material. The characterization reveals a typical micro-mesoporous characteristic with high surface area of 1348.6 cm^2 g^{-1} for MCCN@C material. The micropore sizes centered at 0.58, 0.75 and 1.33 nm, and the mesopore size concentrated at 4.55 and 15.8 nm.

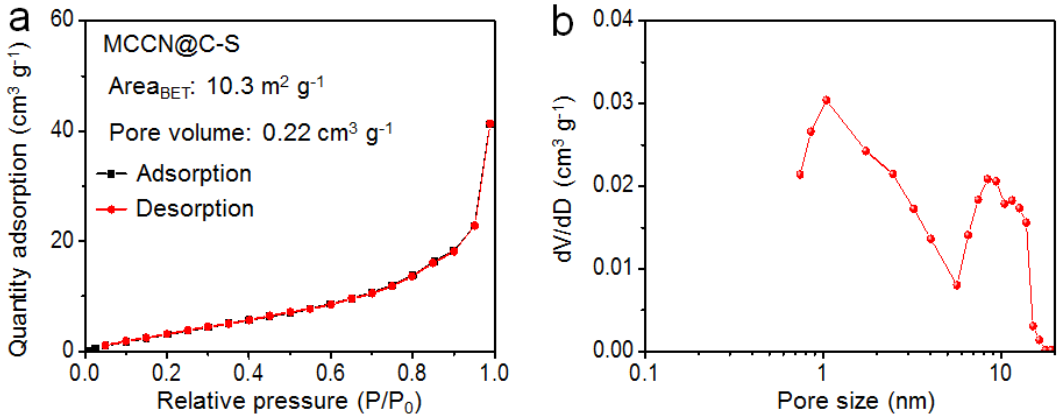

Fig. S7. (a) N_2 adsorption-desorption isotherms and (b) pore size distribution curve of MCCN@C-S composite.

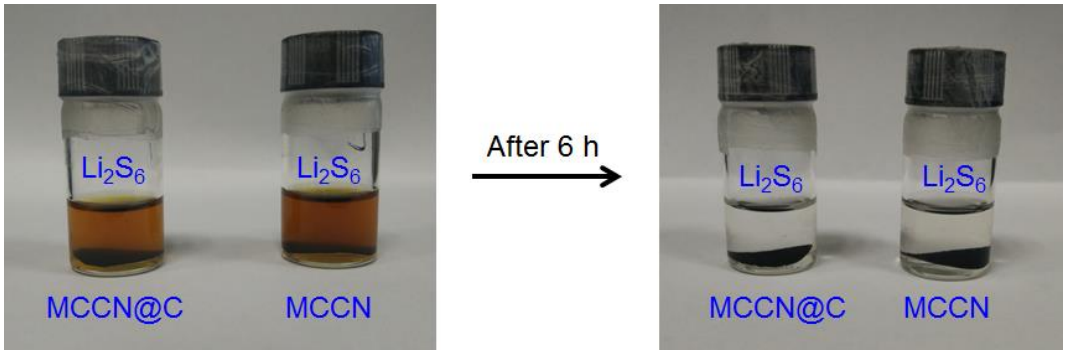

Fig. S8. Adsorption capability tests of MCCN@C and MCCN materials within 0.2 M

Li_2S_6 in DOL/DME solution.

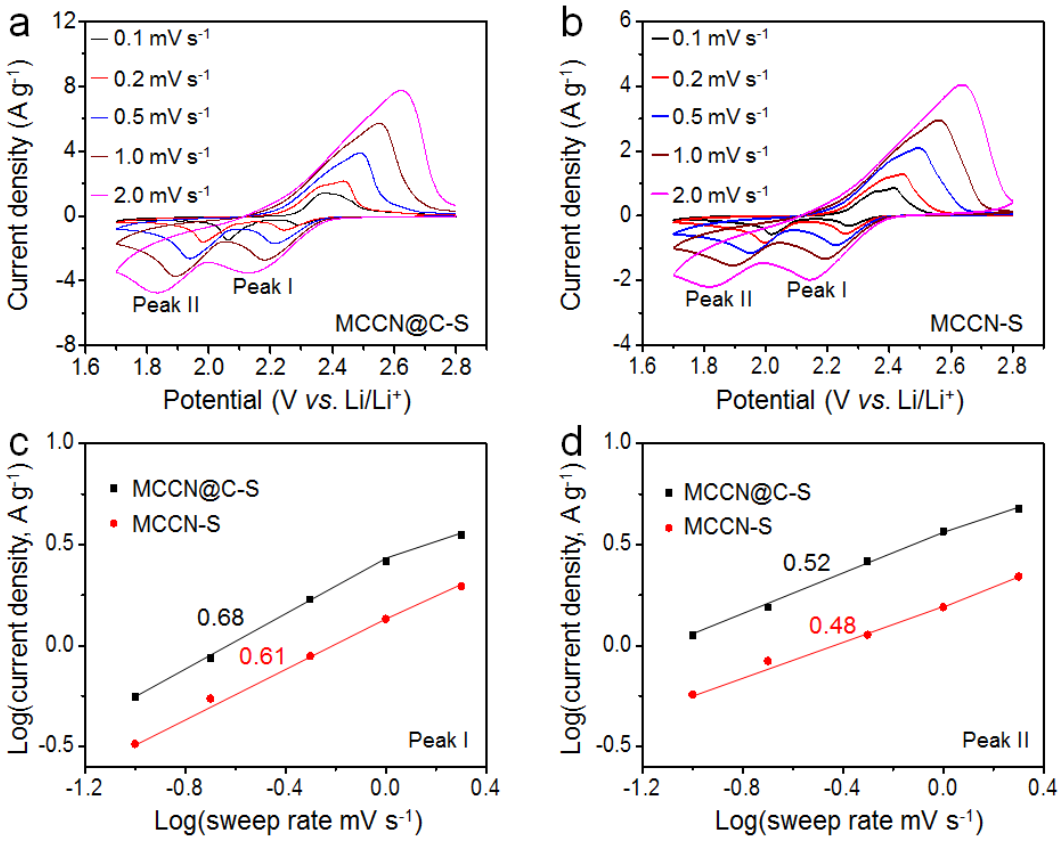

Fig. S9. CV curves of (a) MCCN@C-S and (b) MCCN-S cathodes at different sweep rates. The calculated *b* values from plots of log*i* versus log*v* for (c) peak I and (d) peak II.

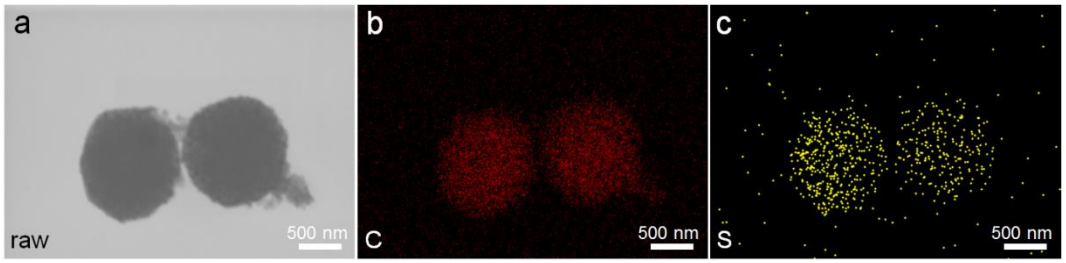

Fig. S10. (a) TEM and (b, c) elemental mapping results of MCCN@C-S after cycling at 0.2 C.

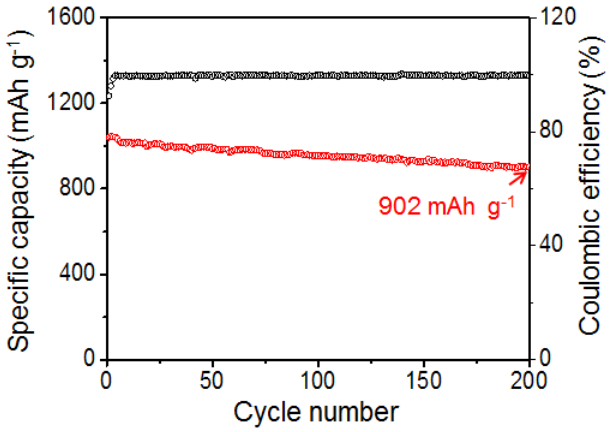

Fig. S11. Cycling performance and the corresponding Coulombic efficiencies of MCCN@C-S cathode with no addition of lithium nitride in electrolyte.

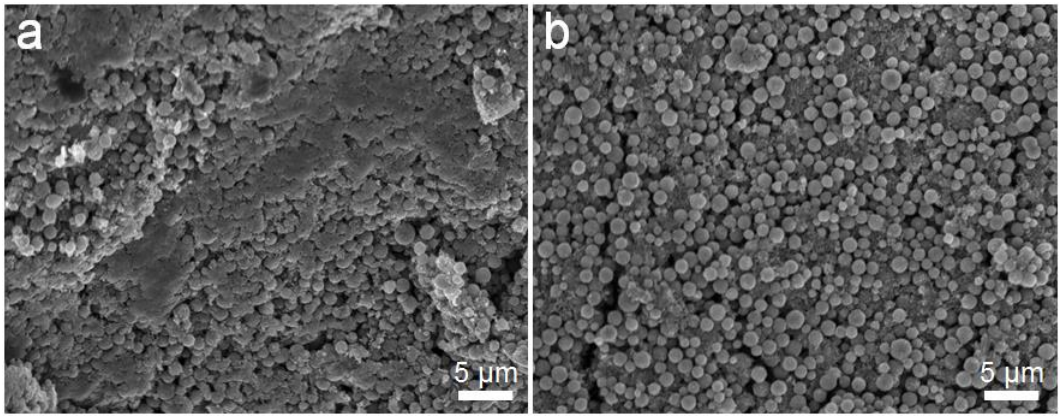

Fig. S12. SEM images of MCCN@C-S cathodes (a) before and (b) after cycling at 2.0 C.